



# Experimental studies of charoite mineral transformations under thermal treatment

A. M. Ionov<sup>1</sup> · O. I. Barkalov<sup>1</sup> · D. A. Shulyatev<sup>2</sup> · K. A. Gavrilicheva<sup>1</sup>

Received: 26 October 2023 / Accepted: 18 April 2024

© The Author(s), under exclusive licence to Springer-Verlag GmbH Germany, part of Springer Nature 2024

## Abstract

Phase transformations of the charoite mineral induced by thermal treatment at high temperatures were studied by simultaneous monitoring of the thermogravimetry, differential scanning calorimetry, and mass spectrometry curves up to its melting temperature range (~ 1300 °C). The chemical composition and phase state of the initial and melted samples were characterized using electron-probe micro-analysis, X-ray photoemission spectroscopy, X-ray powder diffraction, and Raman spectroscopy. It was demonstrated that continuous heating (10 °C/min) up to ~ 500 °C resulting in a mass loss of ~ 5 wt. % was due to crystallization water release and dehydroxylation, while oxygen release and carbonate inclusion decomposition were observed at a higher temperature. The endothermic peak with a heat effect of 82 J/g observed at 970 ÷ 1050 °C was attributed to the charoite-to-wollastonite transition detected by real-time X-ray powder diffraction in this temperature range. Above 1100 °C, another extended endothermic effect was fixed, which was presumably due to the formation of pseudowollastonite and pre-melting processes. The melting of the charoite sample using the floating zone technique resulted in its transformation to pseudowollastonite and caused a significant color change from lilac to rose pink.

**Keywords** Charoite · Thermogravimetry · Calorimetry · X-ray diffraction · Raman spectroscopy · Floating zone melting

## Introduction

Charoite is a delightful mineral, the so-called “lilac miracle of Siberia” (Rogova et al. 2013). This stone is a rare gemstone that is well-known in the gem market due to its exciting aesthetic properties, such as unique lilac to violet color, structural features, and mechanical strength. The main (Russian Federation, Murun massif) deposit “Sirenevyy Kamen” includes both charoite and charoite-containing rocks, with an idealized formula of  $(K, Sr, Ba, Mn)_{15-16}(Ca, Na)_{32}[(Si_{70}(O, OH)_{180})](OH, F)_4 \cdot nH_2O$  (Rozhdestvenskaya et al. 2010), and a complex structure of alkaline calcium silicate with tubular Si–O-radicals  $((Ca_{1.57}Na_{0.51}K_{0.93}Ba_{0.07})_{3.11} \bullet Si_4O_{10}(OH)_{0.58}F_{0.2}O)_{0.78} \bullet 0.72H_2O$ , Rogova et al. 2013). The chemical formula of charoite varies among different outcrops, with inclusions of aegirine, tinaksite, microcline, tokkoite and

some other minerals of the metasomatic rocks also exhibits a complex association (Reguir 2001). The main charoite element components are K, Na, Ca, Si, and O, F, H<sub>2</sub>O, OH, the secondary components are Ba, Sr, and Mn; the presence of traceable amounts of Fe, Mg, Al, Ti, Zr, and Th is discovered in Murun charoite.

The nature of charoite-forming processes has been a subject of scientific discussion. Two major hypotheses have been proposed: a magmatic origin for the charoite-bearing rocks, the charoite rocks crystallised from a fluid-saturated melt. However, the majority of researchers interpret charoites as a typical example of metasomatic rocks (Reguir 2001).

To understand the genesis and properties of charoite it is necessary to study the behavior of the mineral upon its heating to elevated temperatures up to the melting temperature. Moreover, the undoubted interest is to investigate the possibility of charoite crystallization during the melting process. Our study is focused on the high-temperature charoite behavior and the charoite transformation upon melting during crystallization.

✉ A. M. Ionov  
ionov@issp.ac.ru

<sup>1</sup> Osipyan Institute of Solid State Physics of the Russian Academy of Sciences, Chernogolovka, Russia

<sup>2</sup> Materials Modeling and Development Laboratory, NUST MISIS, Leninskiy Prospect, 4, 199049 Moscow, Russia

## Experimental methods and sample characterization

Our experiments were conducted using high-quality samples of charoite. To prepare samples for analysis and melting, samples  $4 \times 4 \times 40$  mm and  $4 \times 4 \times 1$  mm were cut from a mineral block of high jewelry quality, dark lilac-violet color, without visible white, black and yellow inclusions. The content of elements in charoite was determined at IPTM RAS by inductively coupled plasma atomic emission spectrometry (iCAP-6500, Thermo Scientific, USA) and mass spectral methods of analysis (X Series 2, Thermo Scientific, USA). The elemental composition of the samples was characterized before and after thermal treatment by scanning electron microscopy (SEM, Supra 50 VP with EDX detector, Carl Zeiss).

The Raman spectra were recorded with a Princeton Instruments HRS 500 spectrometer equipped with a liquid nitrogen-cooled charge-coupled device detector. The spectra were monitored with 1200 grooves/mm grating. The samples were irradiated at room temperature with a 532-nm KLM-532/SLN-100 DPSS (FTI Optronic, St. Petersburg, Russia) laser with a laser power at the sample of about 5 mW in a back-scattering geometry. A  $20 \times$  Plan Apo Mitutoyo objective was used to focus the laser beam to a spot of approximately  $3 \mu\text{m}$  in size and collect the scattered light. A razor edge Semrock beam splitter and a Holographic Tydex Notch-6 filter (Tydex, St. Petersburg, Russia) were used for laser line discrimination and acquiring the Raman spectra higher than  $200 \text{ cm}^{-1}$ . The spectral resolution in the spectral range under study was  $\approx 1 \text{ cm}^{-1}$ . The spectrometer was calibrated using Ne spectral lines with an uncertainty of  $\pm 1 \text{ cm}^{-1}$ .

The X-ray powder diffraction data (XRD) were taken on Rigaku SmartLab SE, Cu-K $\alpha$  radiation, equipped with 1D D/teX PSD in Bragg–Brentano geometry (Cu-K $\alpha$ 1,2,  $\lambda = 1.5418 \text{ \AA}$ ) at room temperature. The data were collected in a  $2\theta$  range of  $10\text{--}90^\circ$  with a step of  $0.01^\circ$ .

The electron structure and the composition of charoite were studied experimentally by X-ray photoemission spectroscopy (XPS). The high-resolution spectra were measured using a Kratos AXIS Ultra DLD spectrometer with a photon energy of 1486.69 eV, AlK $\alpha$  mono, and the total resolution Ag3d $_{5/2}$  was about 0.48 eV. The spectra were calibrated using Ag3d $_{5/2}$  and C1s lines. The surfaces of the prepared samples were additionally cleaned by argon bombardment in ultra-high vacuum (UHV) in situ. The base pressure during the measurements was in a range of  $5 \cdot 10^{-10}$ – $2 \cdot 10^{-9}$  Torr.

Charoite transformations at high temperatures were studied experimentally upon heating the samples from room temperature to  $1300 \text{ }^\circ\text{C}$  in the air and argon

atmosphere. NETZSCH STA 409 PC/PG was used for simultaneous thermogravimetric and calorimetric analyses from room temperature to a high-temperature of  $1300 \text{ }^\circ\text{C}$  and allowed us to analyze the change in mass, to study the decomposition processes, thermal stability, and behavior during crystallization, and to determine enthalpy transitions, phase transition temperatures. The experiments were performed at a rate of  $10.0 \text{ }^\circ\text{C}/\text{min}$  in an alumina crucible in argon.

Charoite rod were remelted by vertical non-crucible floating zone (FZ) melting with optical radiation heating (Balbashov and Egorov 1981). The charoite rods were FZ melted in the air, the growth rate was  $10\text{--}12 \text{ mm/h}$  at the beginning, and then  $4 \text{ mm/h}$ .

## Results

### Charoite composition

The average chemical composition of the initial sample was SiO $_2$  = 52.29%, CaO = 31.42%, K $_2$ O = 7.60%, Na $_2$ O = 4.23%, BaO = 2.50% (main components, total 98.04%, Supra 50, EDX detector). Element composition is summarized in Table 1.

### Charoite spectroscopy

The XRD powder pattern and Raman spectrum of the initial charoite sample are presented in Fig. 1 and agree well with the experimental data available in the literature (Buzatu and Buzgar 2010; Rozhdestvenskaya et al. 2010; RRUFF R060376).

Only a few studies were made on charoite (Rogova et al. 1978; Rozhdestvenskaya et al. 2009). The Raman spectra for charoite from the RRUFF Project database (Ref. (Downs 2006), R060376) are similar to the spectrum obtained in the present study. No discussions or detailed vibration mode assignments for this mineral were found in the literature. The Raman spectrum of charoite (Fig. 1, right panel) is characterized by strong fluorescence and background, the peaks are very weak, and only a few of them can be resolved. The peak positions are very close to those reported in (Buzatu and Buzgar 2010). An intensive and broad band around  $2400 \text{ cm}^{-1}$  is most probably of luminescence origin. It corresponds to the wavelength of  $\sim 610 \text{ nm}$ , i.e., to the red region of the visible light spectrum.

Typical high-resolution XPS spectra are shown in Fig. 2. The surfaces of the prepared samples were additionally cleaned by argon bombardment in ultra-high vacuum (UHV) in situ.

The elemental composition of the charoite sample was determined by the X-ray photoelectron spectroscopy (XPS)

**Table 1** Elemental composition of the charoite samples

iCAP-6500 and X series 2, Thermo Scientific, USA				
	DL (ppm)	Lilac	Lilac	FZ Melted
Li	0.21	23.1	22.9	19.2
Be	0.21	21.5	16.1	7.18
B	0.79	385	300	<DL
Na	20	–	26000	19236
Mg	2.7	261	226	4.82
Al	200	674	123	21.4
Si	base	320000	309000	278050
K	6	–	48000	69315
Ca	450	190000	155000	158623
Sc	1.1	11.9	12.8	<DL
Ti	23	28.2	21.1	3.03
V	1.6	3.52	31.2	<DL
Cr	0.61	17.9	72.3	<DL
Fe	44	183	186	27.9
Mn	4.2	2709	2540	1904
Co	0.09	0.44	0.55	0.11
Ni	0.34	9.51	9.66	0.43
Cu	0.65	69.9	101	7.07
Rb	0.03	330	306	288
Sr	0.06	8200	7660	23281
Y	0.04	100	80.4	71.2
Zr	0.23	46.7	40.7	36
Nb	0.02	4.82	4.05	3.38
Mo	0.09	0.99	1.24	<DL
Sb	0.09	0.17	0.39	0.014
Cs	0.02	23.7	18.8	16.9
Ba	0.48	36000	30400	38100
La	0.02	463	357	385
Ce	0.04	928	792	944
Pr	0.01	120	88.4	109
Nd	0.02	470	362	384
Sm	0.01	80.4	63.7	64.6
Eu	0.005	18.2	14.1	15.2
Gd	0.02	49.5	39.6	39.1
Tb	0.01	5.26	4.03	4.05
Dy	0.02	23.9	18.5	19.1
Ho	0.003	3.57	2.71	2.9
Er	0.01	8.19	6.31	6.66
Tm	0.002	0.87	0.67	0.75
Yb	0.01	4.75	3.69	3.99
Lu	0.005	0.59	0.42	0.50
Hf	0.32	0.91	0.75	0.86
W	0.02	7.72	6.49	0.038
Pb	2.6	64.1	36.5	19.8
Th	0.05	1.10	0.76	0.91
U	0.01	18.9	14.1	22

DL Detection limit

studies after argon bombardment cleaning with core level lines of the main elements Si2p, Ca2p, Na1s, K2p, Ba3d, Sr3d, O1s, and a weak peak of F1s (Fig. 2b). The photoelectron core level spectra of oxygen O1s and silicon Si2p with binding energies of 530 eV, 532 eV and 104 eV, respectively, were characterized by a typical structure and chemical shift for silicate systems with OH and H<sub>2</sub>O.

### Thermal treatment

The charoite transformation at high temperatures was studied by heating the samples from RT to 1300 °C in argon and the air. First, a lilac-violet charoite sample placed in the alumina or platinum crucibles was heated in the air in a furnace. After heating above 900 °C in the air, the violet color of charoite began to fade, and the sample melted above 1000 °C. These findings probably indicate that the structural transformations of charoite began above 900 °C and agree with the results of (Nikolskaya et al. 1976), where the charoite sample was discolored completely by annealing under the reducing conditions for three hours at 700 °C.

As demonstrated by the mass-spectral curves presented in Fig. 3 (right panel), upon heating, the water release ( $m/e = 17, 18$ ) from the charoite sample occurred in a temperature range of ~50–600 °C, while the release of carbon dioxide ( $m/e = 44$ ) proceeded at 500–800 °C, and that of carbon dioxide and atomic oxygen occurred above ~1000 °C.

The thermogravimetric curve measured upon heating charoite shown in Fig. 3 (left panel) demonstrates singularities at 208, 295, and 460 °C. These values are close to those of our mass spectrometry curves for water ( $m/e = 18$ ) and hydroxyl group ( $m/e = 17$ ), as shown in Fig. 3 (right panel), and those reported in (Matesanz et al. 2008) for the TGA and DTA dependencies. The DSC curve measured in the present work demonstrates a pronounced endothermic shift right above 200 °C and up to ~800 °C. It is featureless in this temperature range probably due to the overlapping of the dehydration, dehydroxylation, and carbonate decomposition processes. A deflection of the first derivative curve of the DSC signal between 500 and 560 °C might point to the peak position of the endothermic processes within this temperature range. The baseline of the DSC signal is more or less leveled above 800 °C, and above 900 °C two endothermic peaks are observed. The former narrow endothermic peak with the onset at ~990 °C and an enthalpy change of 82 J/g should be due to the charoite-to-wollastonite phase transition since the characteristic temperatures determined by the DSC method in the present work coincide with the temperatures obtained by the real-time XRD method and reported in (Janeczek 1991). We assume that the latter broad heat effect fixed above 1100 °C corresponds to the formation of pseudowollastonite from wollastonite and, probably, its premelting. According to the XRD phase analysis

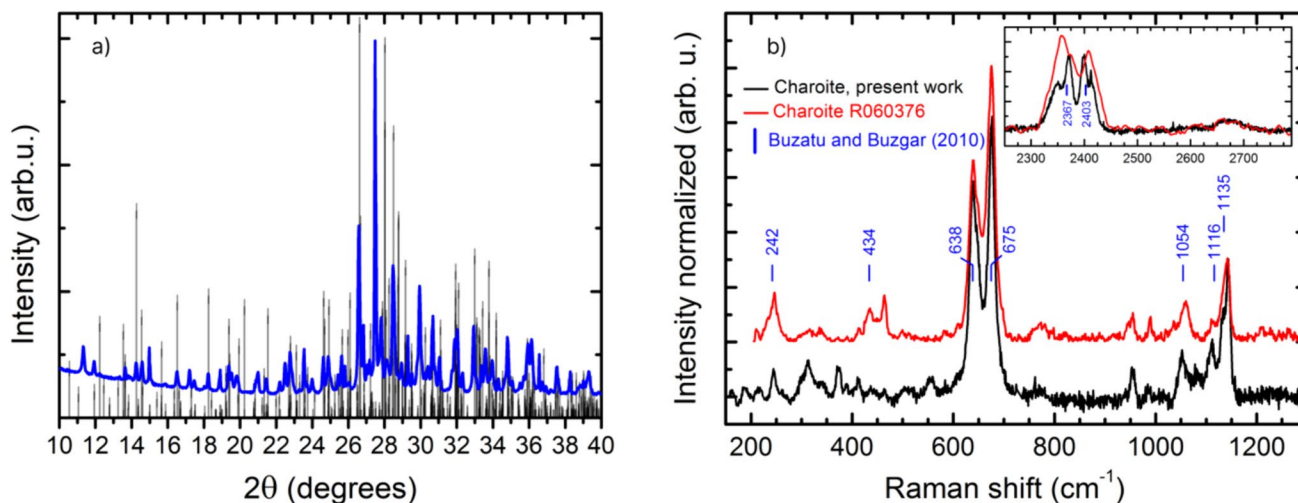


**Fig. 1** The initial charoite sample. **a** The blue curve is X-ray diffraction pattern (CuK $\alpha$ 1 radiation), the black vertical bars represent reflection positions and relative intensities reported in (Rozhdestvenskaya et al. 2010). **b** The representative Raman spectrum of charoite

(black, present work), the Raman spectrum of charoite (red, RRUFF Project database R060376). The inset shows the high-frequency range of the spectra. The blue vertical bars represent the peak positions of the charoite reported in (Buzatu and Buzgar 2010)

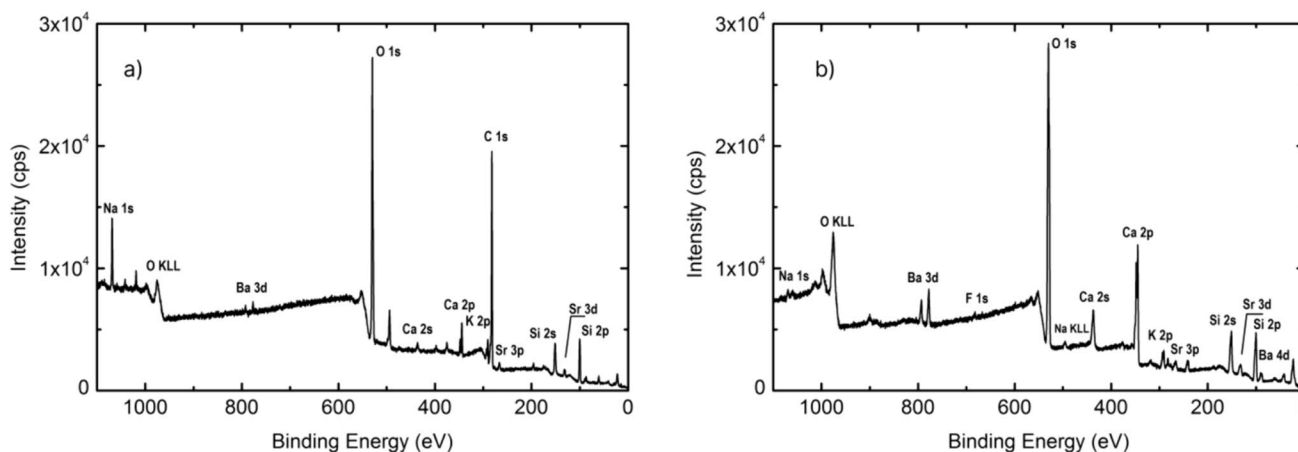


**Fig. 2** High-resolution XPS spectra of the deep lilac-violet mineral sample. **a** as received, **b** the sample surface was cleaned by argon bombardment

of the charoite samples subjected to isochronic annealing (Marchuk et al. 2016), the first traces of the pseudowollastonite phase appeared at  $\sim 1050$  °C and a single phase state was attained at  $\sim 1250$  °C. On the other hand, the synthetic wollastonite CaSiO<sub>3</sub> transforms to pseudowollastonite at 1180 °C (Allen et al. 1906). The melting point of the latter phase is 1512 °C (Allen et al. 1906) or 1547 °C (Richet et al. 1998). The endothermic process is obviously not finished at 1300 °C (see Fig. 3); thus, a calorimeter with a higher temperature limit should be used to get a reliable DSC curve.

Hence, our direct mass-spectral and DSC/TGA experimental data confirm the assumptions on the dehydration and dehydroxylation of charoite upon heating. These assumptions were based on the results of DSC/TG and IR

spectroscopy studies that were reported in (Janeczek 1991; Matesanz et al. 2008; Kaneva et al. 2020).

### Floating zone melting

An attempt to grow a bulk polycrystalline sample of charoite is of undoubted interest, allowing for a reliable characterization of its physical properties and studying the high-temperature transformations of this mineral. Assuming that the growth of charoite crystals should apparently be carried out in a hydrothermal environment, in order to study the behavior of charoite under extreme thermal influences, attempts were made to grow a single crystal using non-crucible zone melting in an oxygen atmosphere. Non-crucible floating



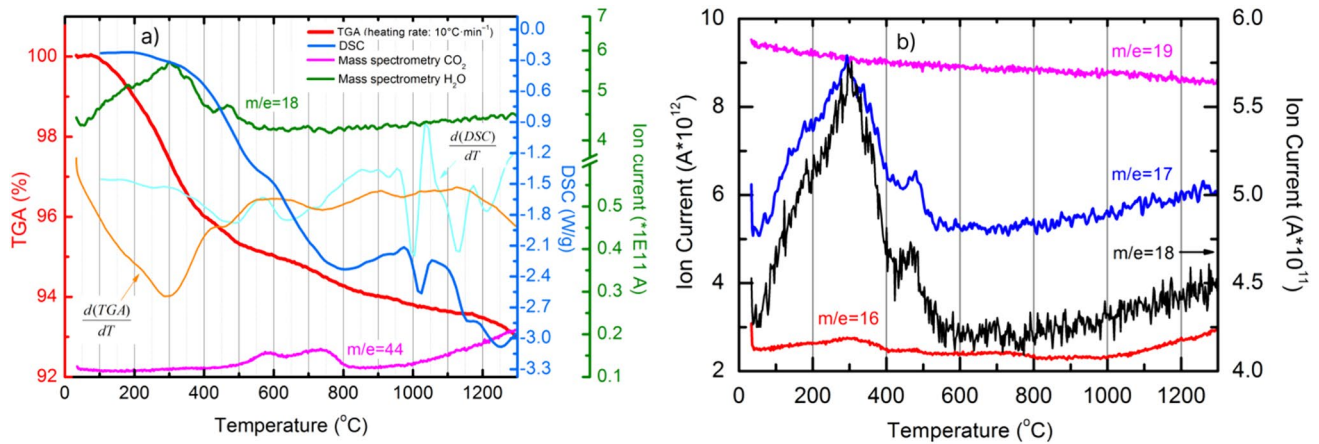


**Fig. 3** **a** DSC (blue) and TGA (red) curves along with the mass spectrometric curve (green H<sub>2</sub>O and magenta CO<sub>2</sub>) for the initial deep violet charoite sample. The light blue and orange curves represent the

first derivatives of the DSC and TGA curves, respectively, in arbitrary units. **b** Mass spectrometric curves: the black curve corresponds to the right ordinate axis, while the others correspond to the left one

zone melting (FZM) with radiation heating is a suitable technique for growing high-quality complex oxide single crystals, as demonstrated in (Balbashov and Egorov 1981; Balbashev et al. 1996).

Charoite rod were remelted by vertical non-crucible floating zone (FZ) melting with optical radiation heating. Rods (4×4×40 mm) for FZ melting were prepared by cutting from the deep violet mineral block. The charoite rods were FZ melted in the air, the growth rate was 10–12 mm/h at the beginning, and then 4 mm/h. At end of melting 70 mm-long whisker was an easily retracted. As a result, the ingot in the form of cylindrical rods of 35–40 mm in length and 3–4 mm in diameter were obtained. The disk-shaped samples with a

thickness of 1 mm and a diameter of 4 mm were prepared by cutting the grown cylindrical rods (see Fig. 4).

The sample color after melting and growth in the air is pale pink-lilac. According to the XRD, there are weak but rather amorphous reflections on the melted part, and the whisker is amorphous. The XRD powder pattern and Raman spectra from central part of ingot of the melted charoite minerals are presented in Fig. 5.

The average chemical composition of the melted sample in the middle part (red line area) is SiO<sub>2</sub> = 62.79%, CaO = 24.16%, K<sub>2</sub>O = 4.28%, Na<sub>2</sub>O = 8.76% (main components, total 99.99%). Elemental composition is summarized in Table 2.

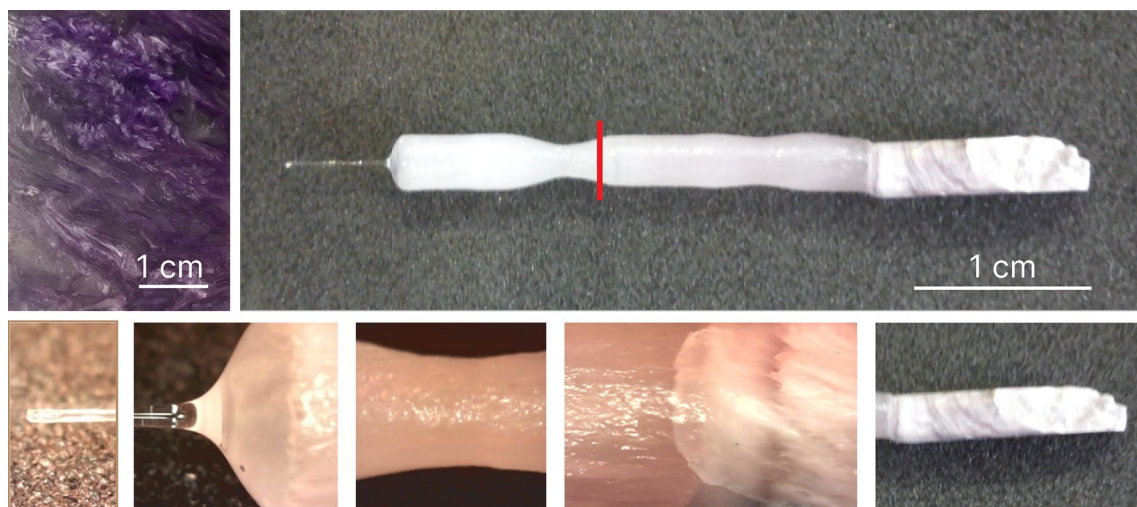


**Fig. 4** Top row: photo of the polished charoite mineral block (left), the cylinder of charoite (about 40 mm in length and 4 mm in diameter) after non-crucible floating zone melting (right). Bottom row: the photos of the cylinder parts on a larger scale

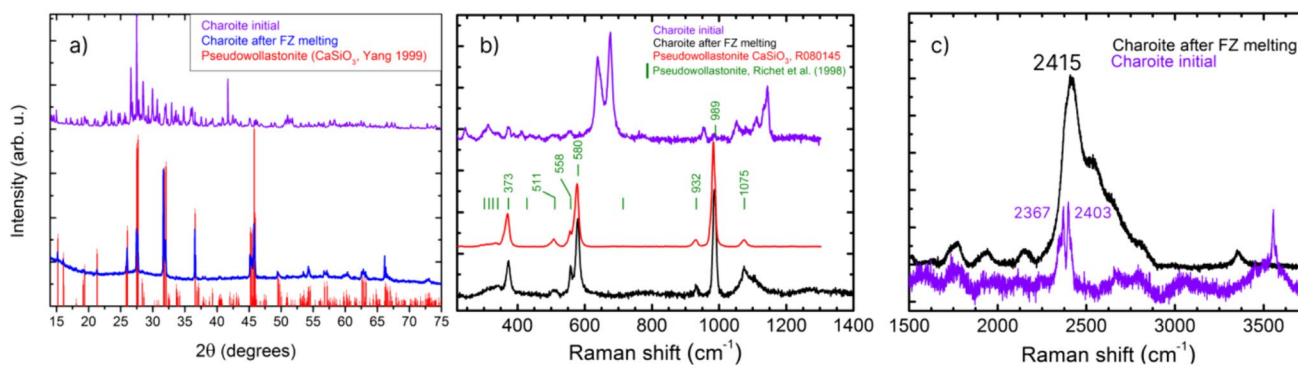


**Fig. 5** The charoite sample after FZ melting. **a** The XRD pattern (violet curve)—initial charoite, blue curve—FZ melted, and the red bars denote positions and intensities for the synthetic pseudowollastonite  $\text{CaSiO}_3$  (Yang and Prewitt 1999). **b** The Raman spectra of the initial charoite sample (violet) and of the charoite sample after FZ melting (black), of the synthetic  $\text{CaSiO}_3$  pseudowollastonite (red,

RRUFF R080145) with the vertical bars denoting the peak positions of the synthetic  $\text{CaSiO}_3$  pseudowollastonite reported in (Richet et al. 1998) and (Chukanov and Vigasina 2020). **c** The high-frequency part of the Raman spectra of the initial charoite sample (violet) and one of the sample after FZ melting (black)

**Table 2** Elemental composition of precursor charoite and Pseudowollastonite composite ingot melted by FZM

Sample melt	Precursor Charoite violet	Precursor Charoite violet	Thin end melted	Thin end melted	Centre melted	Centre melted	Thick end melted	Thick end melted
Element	Weight %	Atomic%	Weight %	Atomic%	Weight %	Atomic%	Weight %	Atomic%
O K	42.26	61.99	50.70	67.27	46.30	63.88	42.63	60.65
Na K	1.37	1.36	3.78	3.52	2.60	2.49	2.06	2.03
Si K	23.78	19.41	25.84	19.74	28.67	22.85	29.94	24.32
K K	6.45	3.78	7.66	4.32	9.80	5.56	10.22	5.94
Ca K	22.83	13.06	8.40	4.55	8.08	4.48	11.33	6.42
Ba L	2.31	0.39	3.62	0.60	4.55	0.74	3.82	0.64

Standard: O— $\text{SiO}_2$ , Na—Albite, Si— $\text{SiO}_2$ , K—MAD-10 Feldspar, Ca—Wollastonite, Ba— $\text{BaF}_2$

Our XRD and Raman data (see Fig. 5) demonstrate the transformation of charoite to high-temperature modification called pseudowollastonite  $\text{Ca}(\text{Na}, \text{K}, \text{Ba})\text{SiO}_3$  having a pale pink color upon melting in the air (see also Table 2). An attempt to grow a single crystal of charoite by non-crucible floating zone (FZ) melting in an oxidizing atmosphere was unsuccessful due to the transformation of charoite into pseudowollastonite and its partial amorphization.

By using the tentative mode assignment made for wollastonite by Buzatu and Buzgar (Buzatu and Buzgar 2010) and for pseudowollastonite by Richet et al. (Richet et al. 1998), the following three frequency ranges might be distinguished in our Raman spectrum of the initial charoite sample (Fig. 1, right) and the pseudowollastonite phase (Fig. 5, right) obtained by the FZ melting procedure. The first one below  $500 \text{ cm}^{-1}$  corresponds to the metal–oxygen stretching modes, the second one,  $500\text{--}850 \text{ cm}^{-1}$ , refers to the O–Si–O bending and Si–O<sub>br</sub> stretching vibrations, and the third one,  $900\text{--}1180 \text{ cm}^{-1}$ , corresponds to the SiO<sub>nbr</sub>

stretching vibrations. However, in the high-frequency region, above  $2300 \text{ cm}^{-1}$  for charoite and above  $1500 \text{ cm}^{-1}$  for pseudowollastonite, a series of peaks is observed with a rather intensive broad band in a range of  $2500\text{--}3000 \text{ cm}^{-1}$ . The latter band is not an overtone of the low-frequency modes; thus, we assume it to be due to luminescence with a wavelength of  $\sim 610 \text{ nm}$ , i.e., in the red region of the visible light spectrum.

## Conclusions

By measuring simultaneously the weight loss (TGA), heat release (DSC), and mass spectrometry (MS) curves upon heating the charoite sample to  $1300 \text{ }^\circ\text{C}$ , we found that the dehydration and dehydroxylation processes (water and hydroxyl group release,  $m/e = 17, 18$ ) occurred at  $50\text{--}460 \text{ }^\circ\text{C}$ . Carbon dioxide release ( $m/e = 44$ ) observed in a temperature range of  $500\text{--}800 \text{ }^\circ\text{C}$  was probably due to decomposition of

the carbonate inclusion in the mineral, and the heated sample lost oxygen ( $m/e = 16$ ) above 1000 °C. The endothermic peak monitored at 970–1055 °C with an integral enthalpy change of 82 J/g was due to the formation of wollastonite from charoite. The melting of charoite by the floating zone procedure resulted in its transition to a pseudowollastonite-like phase.

**Acknowledgements** The authors would like to thank the Shared Facilities Center at the Osipyan Institute of Solid State Physics RAS (Chernogolovka) for the use of the micro-Raman optical system and Rigaku SmartLab SE diffractometer. This work was carried out within the framework of the Governmental Program of Osipyan Institute of Solid State Physics RAS.

**Author contributions** A. I. carried out TGA, DSC and MS experiments, characterized chemical composition and phase state of the samples by means of electron-probe micro-analysis, X-ray photoemission spectroscopy, X-ray powder diffraction and prepared Figs. 1–3 and 5. D.S. conducted FZ melting and prepared Fig. 4. K. G. and O. B. carried out Raman spectroscopy experiment and prepared Figs. 1 and 5. All authors contributed to the writing of the manuscript and reviewed it.

**Data availability** All data is available upon request.

## Declarations

**Conflict of interest** The authors declare that they have no known conflict of financial interest or personal relationships that could have appeared to influence the work reported in this paper.

## References

- Allen ET, White WR, Wright FE (1906) On wollastonite and pseudowollastonite, polymorphic forms of calcium metasilicate, with optical study by F. E. Wright. *Am J Sci* S4-21:89–108. <https://doi.org/10.2475/ajs.s4-21.122.89>
- Balbashov AM, Egorov SK (1981) Apparatus for growth of single crystals of oxide compounds by floating zone melting with radiation heating. *J Cryst Growth* 52:498–504. [https://doi.org/10.1016/0022-0248\(81\)90328-6](https://doi.org/10.1016/0022-0248(81)90328-6)
- Balbashev AM, Shulyatev DA, Panova GK et al (1996) The floating zone growth and superconductive properties of  $\text{La}_{1.85}\text{Sr}_{0.15}\text{CuO}_4$  and  $\text{Nd}_{1.85}\text{Ce}_{0.15}\text{CuO}_4$  single crystals. *Physica C* 256:371–377. [https://doi.org/10.1016/0921-4534\(95\)00647-8](https://doi.org/10.1016/0921-4534(95)00647-8)
- Buzatu A, Buzgar N (2010) The Raman study of single-chain silicates. *Analele Stiintifice ale Universitatii “Al I Cuza” din Iasi Seria Geologie LVI*:107–125
- Chukanov NV, Viggasina MF (2020) *Vibrational (Infrared and Raman) spectra of minerals and related compounds*. Springer International Publishing, Cham
- Downs RT (2006) The RRUFF Project: an integrated study of the chemistry, crystallography, Raman and infrared spectroscopy of minerals. In: RRUFF<sup>TM</sup> Project. <https://rruff.info/>. Accessed 18 Aug 2023
- Janeczek J (1991) Thermal decomposition of charoite. *Mineral Pol* 22:21–27
- Kaneva EV, Radomskaya TA, Shendrik RYu et al (2020) FTIR, XRF and powder XRD experimental study of charoite: crystal chemical features of two associated generations. In: Votyakov S, Kiseleva D, Grokhovsky V, Shchapova Y (eds) *Minerals: structure, properties, methods of investigation*. Springer International Publishing, Cham, pp 97–104
- Marchuk MV, Medvedev VYA, Ivanova LA et al (2016) Charoite experimental studies. *Geodin Tektonofiz* 7:105–118. <https://doi.org/10.5800/GT-2016-7-1-0199>
- Matesanz E, Garcia-Guinea J, Crespo-Feo E et al (2008) The high-temperature behavior of charoite. *Can Mineral* 46:1207–1213. <https://doi.org/10.3749/canmin.46.5.1207>
- Nikolskaya L, Novozhilov A, Samoilovich M (1976) On the nature of colours of the new alkaline calcium silicate from the Eastern Transbaikalia. *Izv AN SSSR*, pp 116–120
- Reguir E. (2001) Aspects of the mineralogy of the Murun alkaline complex, Yakutia, Russia. MSc dissertation, Lakehead University, Ontario, Canada, 2001
- Richet P, Mysen BO, Ingrin J (1998) High-temperature X-ray diffraction and Raman spectroscopy of diopside and pseudowollastonite. *Phys Chem Miner* 25:401–414. <https://doi.org/10.1007/s002690050130>
- Rogova V, Rogov Y, Drits V, Kuznetsova N (1978) Charoite—a new mineral, and a new jewelry stone. *Zap Vses Mineral O-Va* 107:94–100
- Rogova V, Rozhdestvenskaya I, Vorobjov E, et al (2013) Charoite. The Lilac Miracle of Siberia. Illustrated popular science book, 2nd edn. Petrografika, Irkutsk
- Rozhdestvenskaya IV, Kogure T, Abe E, Drits VA (2009) A structural model for charoite. *Mineral Mag* 73:883–890. <https://doi.org/10.1180/minmag.2009.073.2.883>
- Rozhdestvenskaya I, Mugnaioli E, Czank M et al (2010) The structure of charoite,  $(\text{K}, \text{Sr}, \text{Ba}, \text{Mn})_{15-16}(\text{Ca}, \text{Na})_{32}[(\text{Si}_{70}(\text{O}, \text{OH})_{180})](\text{OH}, \text{F})_{4.0}\cdot n\text{H}_2\text{O}$ , solved by conventional and automated electron diffraction. *Mineral Mag* 74:159–177. <https://doi.org/10.1180/minmag.2010.074.1.159>
- Yang H, Prewitt CT (1999) Crystal structure and compressibility of a two-layer polytype of pseudowollastonite ( $\text{CaSiO}_3$ ). *Am Miner* 84:1902–1905. <https://doi.org/10.2138/am-1999-11-1217>

**Publisher's Note** Springer Nature remains neutral with regard to jurisdictional claims in published maps and institutional affiliations.

Springer Nature or its licensor (e.g. a society or other partner) holds exclusive rights to this article under a publishing agreement with the author(s) or other rightsholder(s); author self-archiving of the accepted manuscript version of this article is solely governed by the terms of such publishing agreement and applicable law.